

Article

Macroscopic and Multi-Scale Models for Multi-Class Vehicular Dynamics with Uneven Space Occupancy: A Case Study

Maya Briani ^{1,*}, Emiliano Cristiani ^{1,*} and Paolo Ranut ²

¹ Istituto per le Applicazioni del Calcolo, Consiglio Nazionale delle Ricerche, 00185 Rome, Italy

² Autovie Venete S.p.A., 34143 Trieste, Italy; Paolo.Ranut@autovie.it

* Correspondence: m.briani@iac.cnr.it (M.B.); e.cristiani@iac.cnr.it (E.C.)

Abstract: In this paper, we propose two models describing the dynamics of heavy and light vehicles on a road network, taking into account the interactions between the two classes. The models are tailored for two-lane highways where heavy vehicles cannot overtake. This means that heavy vehicles cannot saturate the whole road space, while light vehicles can. In these conditions, the creeping phenomenon can appear, i.e., one class of vehicles can proceed even if the other class has reached the maximal density. The first model we propose couples two first-order macroscopic LWR models, while the second model couples a second-order microscopic follow-the-leader model with a first-order macroscopic LWR model. Numerical results show that both models are able to catch some second-order (inertial) phenomena such as stop and go waves. Models are calibrated by means of real data measured by fixed sensors placed along the A4 Italian highway Trieste–Venice and its branches, provided by Autovie Venete S.p.A.

Keywords: LWR model; follow-the-leader model; phase transition; creeping; seepage; fundamental diagram; lane discipline; networks

MSC: 35L65; 35F25; 90B20; 76T99



Citation: Briani, M.; Cristiani, E., Ranut, P. Macroscopic and Multi-Scale Models for Multi-Class Vehicular Dynamics with Uneven Space Occupancy: A Case Study. *Axioms* **2021**, *10*, 102. <https://doi.org/10.3390/axioms10020102>

Academic Editor: Angel R. Plastino

Received: 31 March 2021

Accepted: 15 May 2021

Published: 24 May 2021

Publisher's Note: MDPI stays neutral with regard to jurisdictional claims in published maps and institutional affiliations.



Copyright: © 2021 by the authors. Licensee MDPI, Basel, Switzerland. This article is an open access article distributed under the terms and conditions of the Creative Commons Attribution (CC BY) license (<https://creativecommons.org/licenses/by/4.0/>).

1. Introduction

In this paper, we deal with macroscopic and multi-scale modeling of traffic flow on a road network, focusing on multi-class dynamics which couple light and heavy vehicles (in the following, cars and trucks). The proposed models are characterized by the fact that cars and trucks interact with each other and that trucks are confined to a part of the road space (slow lane) and cannot overtake. As a consequence, when trucks saturate the space and form a queue, cars can still move, although at reduced speed.

1.1. State of the Art

The literature about traffic flow is very large and many different aspects of traffic dynamics were described through mathematical models. Let us start from classic approaches: in a single-lane *microscopic* (agent-based) framework with N vehicles and no overtaking, each vehicle $k \in \{1, \dots, N\}$ is singularly identified by its position $X_k(t)$ and its velocity $V_k(t)$. By assumption, the $(k + 1)$ -th vehicle is always in front of the k -th one. Further, each vehicle is assumed to adjust its acceleration based on the difference in positions and velocities between the vehicle itself and the vehicle in front of it. This approach leads to the following system of ordinary differential equations:

$$\begin{cases} \dot{X}_k = V_k \\ \dot{V}_k = A(X_k, X_{k+1}, V_k, V_{k+1}) \end{cases}, \quad k = 1, \dots, N - 1 \quad (1)$$

where A is a given acceleration function. The first vehicle in the row ($k = N$), called *leader*, has an independent dynamics. Since the whole dynamics is determined by the leader's one through a domino effect, these kinds of models are known as follow-the-leader.

Adopting, instead, a *macroscopic* (fluid dynamics) point of view, we describe the mass of vehicles by means of their density $\rho(x, t)$ only. The celebrated LWR model [1,2] is based on the observation that the density ρ evolves in time, ruled by the following conservation law:

$$\partial_t \rho + \partial_x f(\rho) = 0, \quad x \in \mathbb{R}, \quad t > 0 \quad (2)$$

where the function $f(\rho)$, called *fundamental diagram*, is given and represents the flux of vehicles as a function of the density itself. The velocity of the vehicles can be recovered from ρ thanks to the relation

$$v(\rho) = \frac{f(\rho)}{\rho}, \quad (\rho \neq 0). \quad (3)$$

It is important to note that the microscopic model (1) is second-order, i.e., acceleration-based, while the macroscopic model (2) is first-order, i.e., velocity-based. The difference is important because velocity-based models, allowing nonphysical instantaneous accelerations, are not able to catch effects caused by inertia, such as stop and go waves. Due to this difference, it is plain that the model (2) is not the many-particle limit of the model (1). We refer the interested reader to [3] for a review of various many-particle limits (i.e., micro-to-macro correspondences) and the existing multi-scale models.

The first generalization of the models (1) and (2) of our interest is that of *road networks*. While managing junctions in microscopic models is relatively easy, doing the same in a macroscopic setting is more challenging. The reason is that, in general, the conservation of the mass alone is not sufficient to characterize a unique solution at junctions. We refer the reader to the book by Garavello and Piccoli [4] for more details about the ill-posedness of the problem at junctions. Multiple workarounds for such ill-posedness have been suggested in the literature: (i) maximization of the flux across junctions and introduction of priorities among the incoming roads [4–6]; (ii) introduction of a *buffer* to model the junctions by means of an additional ordinary differential equation coupled with (2) [7–9]; (iii) reformulation of the problem on all possible paths on the network rather than on roads and junctions. The last approach has both a global formulation [10–12] and a more manageable local formulation, described in [13], which is the one we will adopt in this paper. All these approaches allow determining a unique solution for the traffic evolution on the network, but the solutions might be different.

The second generalization of our interest is that of *multi-class* dynamics. “Multi-class” is a very generic term used in the literature to refer to the case in which the road is populated by different groups of vehicles/drivers, and tracking each group separately is desired. Again, doing this in a microscopic framework is easy since it is sufficient to label each vehicle on the basis of the class it belongs to. In the macroscopic setting, instead, we need to introduce as many density functions as there are classes and then establish the interactions between classes. This leads to a system of conservation laws of the form

$$\partial_t \rho_c + \partial_x f_c(\rho_1, \dots, \rho_C) = 0, \quad c = 1, \dots, C, \quad x \in \mathbb{R}, \quad t > 0 \quad (4)$$

where C is the number of classes, $c \in \{1, \dots, C\}$, ρ_c is the density of class c and f_c is the flux of class c which depends on all densities (usually the dependence is on the sum of all densities $\sum_c \rho_c$). Multi-class models are used to describe very different situations, such as the co-presence of vehicles with

- Different driving modes (e.g., autonomous vs. classic);
- Different origins and destinations;
- Different lengths (i.e., space occupied);
- Different velocities/flux functions;

- Reserved roads or reserved entry/exit lanes.

A complete review of multi-class models is out of the scope of this paper. We refer to [14–16] and to the recent books [17,18] for an overview of the most used multi-class models.

Before introducing our contributions, let us introduce the *creeping or seepage effect* [14,19] which will be useful to describe the features of the proposed models. This term denotes the situations where the road space is shared by small and large vehicles, and small vehicles are able to move (at reduced velocity) even if large vehicles have reached the maximal density. This is in contrast to classical models such as the one proposed by Benznoni-Gavage and Colombo [20], in which the saturation of a class of vehicles immediately stops all the other classes. It is useful to note that the creeping phenomenon is typically considered in a context of *disordered traffic*, i.e., traffic with no lane discipline: smaller vehicles (e.g., two wheels) slip into the empty spaces left by large vehicles, similar to motion through porous media. This is not the case considered here, since we assume a strict lane discipline.

Finally, let us recall some important contributions about the fundamental diagram and its properties. It is well known that a single function $f = f(\rho)$ is not able, alone, to describe real data correctly. Indeed, by (3), we deduce that for any given density value ρ , only one velocity $v(\rho)$ is possible. This is not what happens in reality, where a scattered fundamental diagram is observed instead, due to the fact that different drivers respond in a different way to the same traffic conditions. Many papers investigated this phenomenon from different points of view, trying to explain its features, including instabilities; see, e.g., [21–31].

1.2. Case Study

In this paper, we consider the Italian motorway A4 Trieste–Venice and its branches to/from Udine, Pordenone and Gorizia, managed by Autovie Venete S.p.A., see Figure 1.



Figure 1. The Italian motorway A4 Trieste–Venice and its branches to/from Udine, Pordenone and Gorizia, managed by Autovie Venete S.p.A.

At the time of the present study (2019), the motorway had two lanes per direction, except for the leftmost segment near Venice (Venice–San Donà). To avoid heterogeneous conditions, we dropped the three-lane segment of the road to focus exclusively on the parts with *two lanes per direction*. In those segments, cars can use both lanes at any time, while trucks can use only the slow lane and cannot overtake. Due to the large flow of heavy vehicles, it happens sometimes that a queue of trucks is formed. In this case, cars move into the fast lane and keep going, although at moderate speed. When traffic conditions are sustained, the two classes of vehicles interact with each other: on the one hand, trucks act as moving bottlenecks for cars (cf. [32]), which are forced to slow down due to the

restricted space; on the other hand, trucks must slow down when cars find it convenient to occupy part of the slow lane.

1.3. Our Contribution

In this paper, we propose two models for describing multi-class traffic flow on networks in which vehicles belonging to different classes share the road space only partially. More precisely, light vehicles can occupy the whole road, while heavy vehicles can occupy only a part of it. To align with the case study, we will assume that the road has two lanes in total and trucks can occupy only the slow one, without overtaking.

1. The first model is purely macroscopic. Both cars and truck are described by two coupled first-order LWR-based models. Fundamental diagrams are shaped in order to allow cars to move even in the presence of fully congested trucks. Considering that the fundamental diagram of each class is influenced by the presence of the other class, in the case of unstable (rapidly varying) traffic conditions of one class, we observe a scattered behavior in the fundamental diagram of the other class. Numerical results will show that this feature allows the model to catch, at least in part, some second-order (inertial) phenomena in traffic behavior, such as stop and go waves.
2. The second model is multi-scale. Cars are described by a first-order LWR-based model, while trucks are described by a second-order microscopic follow-the-leader model. For trucks, we consider the microscopic model used in [3], inspired, in turn, by a model originally proposed in [33] and specifically designed to reproduce stop and go waves. The choice of second-order model for trucks is crucial, since inertia effects are not at all negligible for those vehicles, while they are less important in car dynamics. Finally, note that, since trucks are confined to only one lane and cannot overtake, their dynamics perfectly matches the constituting assumptions of the follow-the-leader model.

Let us finally mention that the idea of coupling first- and second-order models was already exploited in [3] in a single-class scenario.

Remark 1. *Both models distinguish classes, but not lanes. The fact that trucks cannot use the fast lane while cars can occupy both slow and fast lanes is encapsulated in the choice of the fundamental diagrams.*

2. Dataset

Autovie Venete constantly monitors traffic conditions by means of video cameras, mobile sensors and fixed sensors. In this paper, we focus on the latest kind of data. Fixed sensors are located along the motorway, on each lane, and measure the flux and velocity of all vehicles passing in front of them, also distinguishing the class of vehicles. Data are aggregated per minute and are stored in a database for later analysis. For light vehicles, we further aggregated data coming from slow and fast lanes. For heavy vehicles, instead, we considered the slow lane only. In Figures 2–4, we show some flux and velocity data coming from some fixed sensors, used to conceive and calibrate the models presented in this paper. For better readability, flux data are plotted as both raw (as is) and smoothed by a Gaussian filter. Note that the flux data are always a multiple of 60 since they are evaluated every minute, but they are expressed in terms of vehicles per hour.

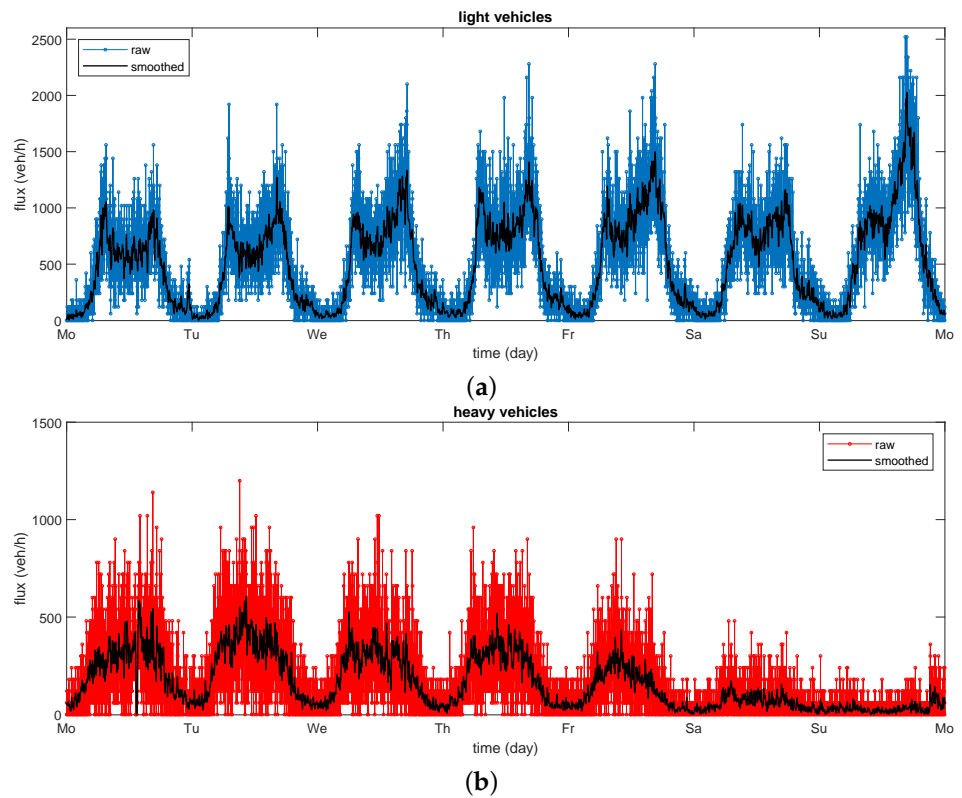


Figure 2. Typical weekly (from Monday to Sunday) flux data on the A4 motorway of (a) light and (b) heavy vehicles collected on March 2019 near Redipuglia. Smoothed data are plotted in black. Note the flux drop of cars in the middle of the day and of trucks on the weekend.

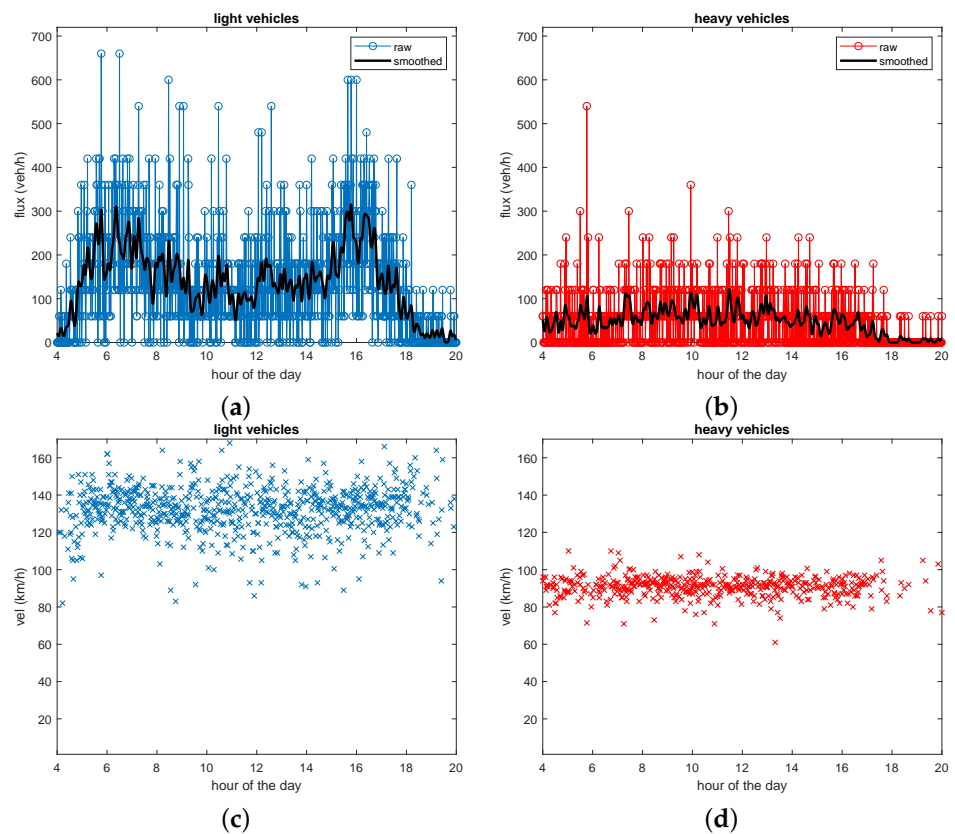


Figure 3. Typical daily (Thursday) flux and velocity data on the A28 motorway of (a–c) light and (b–d) heavy vehicles collected in May 2019 near Sesto al Reghena.

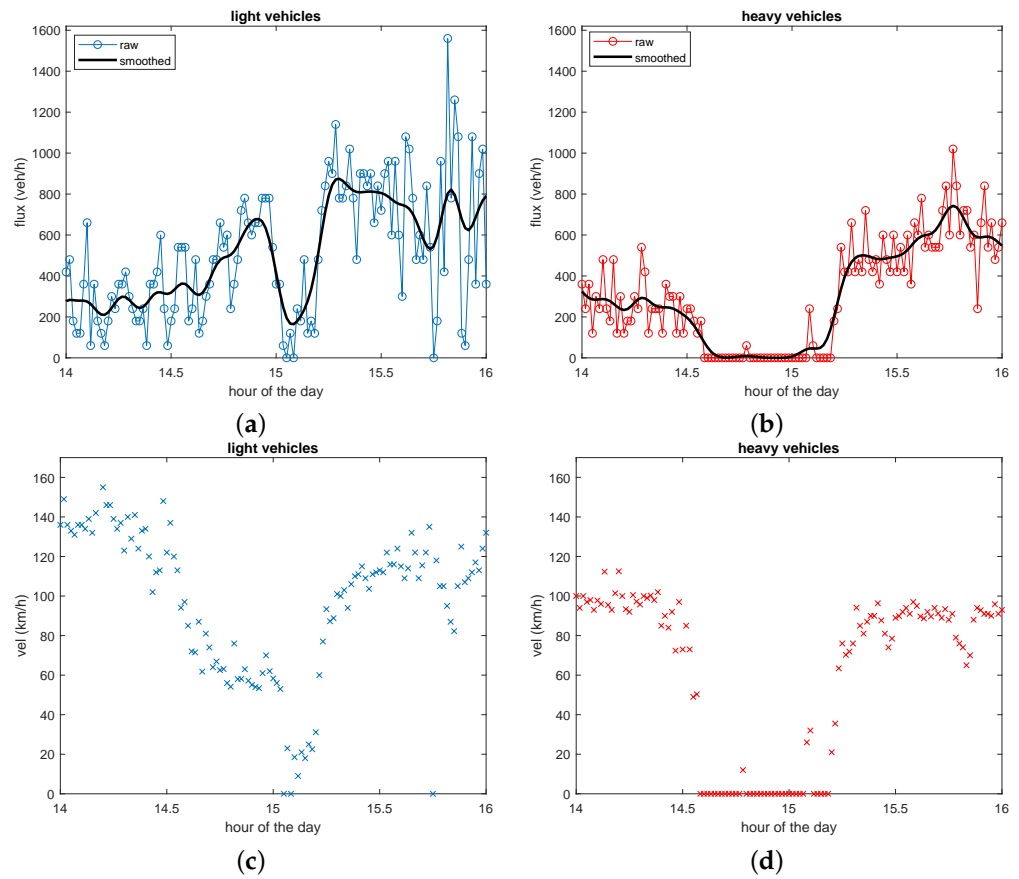


Figure 4. Creeping phenomenon registered in May 2019 near Portogruaro: (a) Light vehicles move in the fast lane even if (b) heavy vehicles queue in the slow lane. (c) Light vehicles’ velocity drops from ~140 to ~60 km/h and then to ~20 km/h while (d) heavy vehicles are completely stopped.

3. Models

In this section, we present the two models. As already stated in the Introduction, the models are not meant to provide the same results or to be the many-particle limit of the other. Nevertheless, they share the most important constitutive assumptions, and for this reason, they are expected to provide the same qualitative results. The most important common modeling assumption is that the car dynamics is influenced, at any time, by the presence of trucks, while the truck dynamics is affected by cars only if the density of cars exceeds a certain threshold, which corresponds to the fact that cars cannot be confined to the fast lane any longer and must invade the slow lane where trucks live. This assumption comes from an important piece of evidence: cars tend to avoid being trapped between two trucks in the slow lane and prefer moving to the fast lane. Doing this, cars move to the side of trucks (overtaking them if possible) and do not affect their dynamics, unless the density of cars is so high that they must necessarily occupy the slow lane too.

3.1. Macroscopic Model

We denote by ℓ_L and by ℓ_H the average length of light vehicles (cars) and heavy vehicles (trucks), respectively, and we define

$$\beta := \frac{\ell_L}{\ell_H} < 1. \tag{5}$$

We also denote by ρ_L the density of cars and by ρ_H the density of trucks. Similarly, we denote by ρ_L^{\max} and ρ_H^{\max} the maximal densities for cars and trucks, respectively. They are defined as

$$\rho_L^{\max} = \frac{2}{\ell_L} \quad \text{and} \quad \rho_H^{\max} = \frac{1}{\ell_H}, \tag{6}$$

having assumed that there are two available lanes for cars and only one for trucks. Note that density values are expressed in terms of number of vehicles per unit of space. Considering that trucks occupy more space than cars, a direct comparison of the two densities is not meaningful. For this reason, the two classes are typically compared in terms of occupied space.

The two-class dynamics is physically admissible if the two densities fall in the set

$$\mathcal{D} := \left\{ (\rho_L, \rho_H) : 0 \leq \rho_L \leq \rho_L^{\max}, 0 \leq \rho_H \leq \rho_H^{\max}, 0 \leq \rho_L + \frac{\rho_H}{\beta} \leq \rho_L^{\max} \right\}, \tag{7}$$

which is well defined if $\rho_L^{\max} - \frac{\rho_H^{\max}}{\beta} \geq 0$. In the following, in order to cope with the uneven space occupancy, we assume that the last condition is verified with the strict inequality

$$\rho_L^{\max} - \frac{\rho_H^{\max}}{\beta} > 0. \tag{8}$$

We consider the following two-class model for $(\rho_L, \rho_H) \in \mathcal{D}$:

$$\begin{cases} \partial_t \rho_L + \partial_x f_L(\rho_L, \rho_H) = 0 \\ \partial_t \rho_H + \partial_x f_H(\rho_L, \rho_H) = 0 \end{cases} \quad x \in \mathbb{R}, \quad t > 0, \tag{9}$$

where

$$f_L(\rho_L, \rho_H) := \rho_L v_L(\rho_L, \rho_H), \quad f_H(\rho_L, \rho_H) := \rho_H v_H(\rho_L, \rho_H)$$

define the two fundamental diagrams and v_L, v_H are the speed functions for light and heavy vehicles, respectively. We then have a family of flow–density curves $\rho_L \mapsto f_L(\rho_L, \rho_H)$ for cars, parameterized by the truck density ρ_H , and, analogously, a family of flow–density curves $\rho_H \mapsto f_H(\rho_L, \rho_H)$ for trucks, parameterized by ρ_L .

We assume that the flux and speed functions satisfy the following properties:

(L1) $v_L(\rho_L, \rho_H) \geq 0$ for all $(\rho_L, \rho_H) \in \mathcal{D}$ and $v_L(\rho_L, \rho_H) = 0$ iff $\rho_L = \rho_L^*(\rho_H)$, where

$$\rho_L^*(\rho_H) := \rho_L^{\max} - \rho_H / \beta \tag{10}$$

is the maximum admissible car density given the truck density ρ_H ;

(L2) $v_L(\rho_L, \rho_H)$ is a decreasing function with respect to ρ_L and ρ_H ;

(L3) $f_L(0, \rho_H) = 0$ and $f_L(\rho_L^*(\rho_H), \rho_H) = 0$ for all $\rho_H \in [0, \rho_H^{\max}]$;

(L4) $f_L(\rho_L, \rho_H)$ is concave with respect to ρ_L for any ρ_H . We define

$$\sigma_L(\rho_H) := \arg \max_{\rho_L} f_L(\rho_L, \rho_H) \tag{11}$$

which represents, as usual, the interface between freeflow and congested regimes;

(L5) $f_L(\rho_L, \rho_H)$ is a decreasing function with respect to ρ_H for any ρ_L .

Similarly,

(H1) $v_H(\rho_L, \rho_H) \geq 0$ for all $(\rho_L, \rho_H) \in \mathcal{D}$ and $v_H(\rho_L, \rho_H) = 0$ iff $\rho_H = \rho_H^*(\rho_L)$, where

$$\rho_H^*(\rho_L) := \min\{\rho_H^{\max}, \beta(\rho_L^{\max} - \rho_L)\} \tag{12}$$

is the maximum admissible truck density given the car density ρ_L ;

(H2) $v_H(\rho_L, \rho_H)$ is a decreasing function with respect to ρ_L and ρ_H ;

(H3) $f_H(\rho_L, 0) = 0$ and $f_H(\rho_L, \rho_H^*(\rho_L)) = 0$ for all $\rho_L \in [0, \rho_L^{\max}]$;

(H4) $f_H(\rho_L, \rho_H)$ is concave with respect to ρ_H for any ρ_L . We define

$$\sigma_H(\rho_L) := \arg \max_{\rho_H} f_H(\rho_L, \rho_H) \tag{13}$$

which represents, as usual, the interface between freeflow and congested regimes;

(H5) $f_H(\rho_L, \rho_H)$ is a decreasing function with respect to ρ_L for any ρ_H .

To cope with the peculiarities of the dynamics, we consider a *phase transition* (cf. [34–36]) caused by the presence of two states of the system:

- The *partial coupling phase* is in place when

$$(\rho_L, \rho_H) \in \mathcal{D}_1 := \left\{ 0 \leq \rho_H \leq \rho_H^{\max}, 0 \leq \rho_L \leq \rho_L^{\max} - \rho_H^{\max} / \beta \right\}, \tag{14}$$

see Figure 5.

In this phase, we assume that cars are mainly in the fast lane and do not affect the truck dynamics. Trucks are then independent from cars.

For trucks, we choose a triangular fundamental diagram with

$$v_H(\rho_H) = V_H^{\max} \quad \text{for all } \rho_H \leq \sigma_H, \tag{15}$$

where V_H^{\max} is the maximum speed of trucks, see Figure 6b.

Cars do not interfere with trucks but adapt their dynamics to the presence of them. Moreover, for cars, we choose (a family of) triangular fundamental diagrams, see Figure 6a. Specifically, we set

$$v_L(\rho_L, \rho_H) = \begin{cases} V_L^*(\rho_H) & \text{if } \rho_L \leq \sigma_L(\rho_H), \\ \frac{V_L^*(\rho_H) \sigma_L(\rho_H)}{\rho_L^*(\rho_H) - \sigma_L(\rho_H)} \left(\frac{\rho_L^*(\rho_H)}{\rho_L} - 1 \right) & \text{if } \sigma_L(\rho_H) < \rho_L \leq \rho_L^{\max} - \rho_H^{\max} / \beta, \end{cases} \tag{16}$$

where $V_L^*(\rho_H)$ is the maximum speed of cars given the truck density. We also define $V_L^*(0) = V_L^{\max}$ as the maximum speed of cars in the absence of trucks. Then, $V_L^*(\rho_H) \geq 0$ and $\sigma_L(\rho_H) \geq 0$ are continuous linear decreasing functions of ρ_H .

For $(\rho_L, \rho_H) \in \mathcal{D}_1$, the model (9) then becomes

$$\begin{cases} \partial_t \rho_L + \partial_x f_L(\rho_L, \rho_H) = 0 \\ \partial_t \rho_H + \partial_x f_H(\rho_H) = 0 \end{cases} \tag{17}$$

where $f_L(\rho_L, \rho_H) = \rho_L v_L(\rho_L, \rho_H)$ and $f_H(\rho_H) = \rho_H v_H(\rho_H)$, as described in Figure 6.

- The *full coupling phase* is in place when $(\rho_L, \rho_H) \in \mathcal{D}_2 := \mathcal{D} \setminus \mathcal{D}_1$, see Figure 5. In this case, we assume that there are too many cars to find it convenient to be confined to the fast lane. For this reason, they invade the slow lane, thus influencing the dynamics of trucks. The two equations in system (9) are then fully coupled.

As before, we choose for both classes a family of triangular fundamental diagrams which extend, by continuity, those defined in \mathcal{D}_1 , as shown in Figure 7.

We define the *transition level* as the threshold density of light vehicles which acts as an interface between the two phases, see Figure 5. In our setting, trucks are confined to one of the two available lanes, and then the transition level is equal to $\rho_L^{\max} - \rho_H^{\max} / \beta = \rho_L^{\max} / 2$.

Note also that the fundamental diagrams we use in this work verify all the properties (L1)–(L5) and (H1)–(H5).

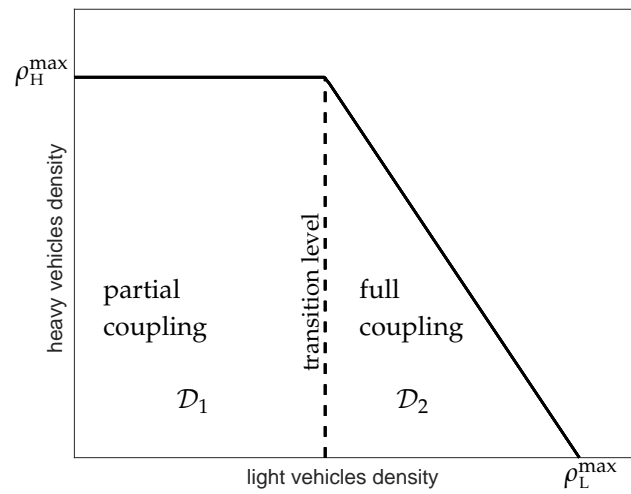


Figure 5. Domains \mathcal{D}_1 and \mathcal{D}_2 of the macroscopic model (9).

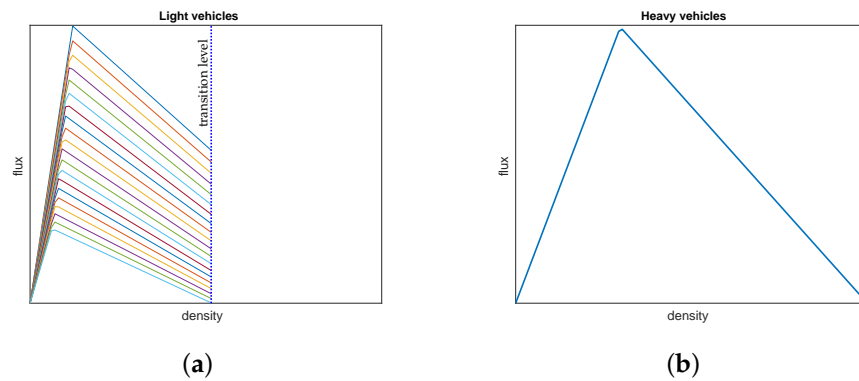


Figure 6. Fundamental diagrams of the macroscopic model in the partial coupling phase, i.e., $(\rho_L, \rho_H) \in \mathcal{D}_1$. (a) Light vehicles, (b) heavy vehicles.

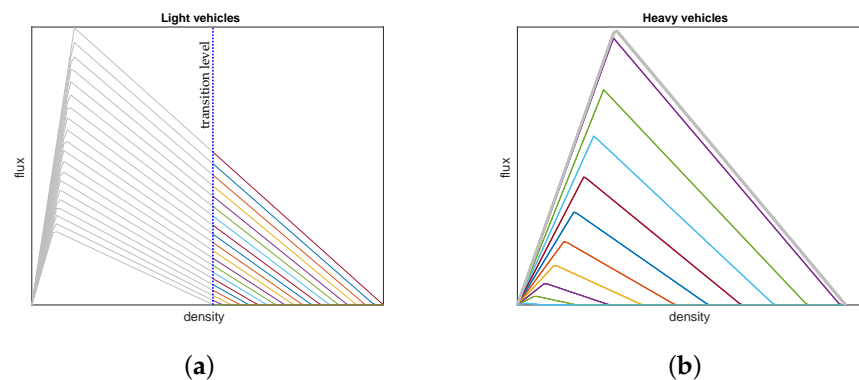


Figure 7. Fundamental diagrams of the macroscopic model in the full coupling phase, i.e., $(\rho_L, \rho_H) \in \mathcal{D}_2$. (a) Light vehicles, (b) heavy vehicles.

3.2. Multi-Scale Model

In this section, we describe the multi-scale model. Here, cars are described by a first-order LWR model of type (2), and trucks are described by a second-order microscopic follow-the-leader model of type (1). Let us describe the microscopic model first, dropping, for the moment, the coupling with light vehicles.

3.2.1. Microscopic Model for Heavy Vehicles

The microscopic model is the one presented in [3], which is, in turn, inspired by the model originally proposed by Zhao and Zhang in [33].

In the following, we denote by Δ_k the gap between truck k and truck $k + 1$ at any time t :

$$\Delta_k(t) := X_{k+1}(t) - X_k(t).$$

It is plain that this gap is inversely proportional to the density of heavy vehicles. We define in (1)

$$A(X_k, X_{k+1}, V_k, V_{k+1}) = \begin{cases} \frac{1}{\tau_{acc}} \left(v^{ZZ}(\Delta_k) - V_k \right), & \text{if } v^{ZZ}(\Delta_k) \geq V_k \\ \frac{1}{\tau_{dec}} \left(v^{ZZ}(\Delta_k) - V_k \right), & \text{if } v^{ZZ}(\Delta_k) < V_k \end{cases} \quad (18)$$

where the function v^{ZZ} represents the equilibrium velocity all drivers tend to and depends on the gap Δ_k . Parameters $\tau_{acc}, \tau_{dec} > 0$ are the relaxation times as usual, differentiated for the acceleration and the deceleration phase. Diversifying the relaxation times appeared to be crucial to fit real data.

The velocity function v^{ZZ} is defined by

$$v^{ZZ}(\Delta) := \begin{cases} 0, & \text{if } \Delta \leq \Delta_{close} \\ \frac{V_H^{max}}{\Delta_{far} - \Delta_{close}} (\Delta - \Delta_{close}), & \text{if } \Delta_{close} < \Delta < \Delta_{far} \\ V_H^{max}, & \text{if } \Delta \geq \Delta_{far} \end{cases} \quad (19)$$

where $\Delta_{close}, \Delta_{far}, V_H^{max}$ are positive parameters, see Figure 8.

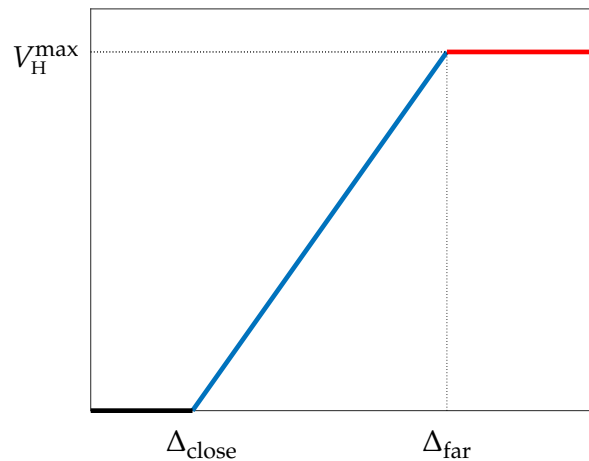


Figure 8. The shape of the velocity function $v^{ZZ}(\Delta)$ defined in (19).

The plateau in $\Delta \in [0, \Delta_{close}]$ is crucial for correctly reproducing stop and go waves. Indeed, once the relaxation times τ_{acc}, τ_{dec} are fixed, the capability of the model to trigger stop and go waves is ruled precisely by Δ_{close} .

3.2.2. Full Model

First of all, given the parameter $\delta > 0$, we assume that cars located at x are influenced by a truck iff the distance between the truck and x is less than δ . We denote the number of trucks falling in the road interval $[x - \delta, x + \delta)$ at any time t by

$$N_H^\delta(x, t) := \#\{k : X_k(t) \in [x - \delta, x + \delta)\}. \quad (20)$$

Second, we denote by ρ_L the density of light vehicles and by v_L their velocity. To couple the dynamics of the two classes, we assume that v_L depends on both ρ_L (as in the

classical LWR model) and N_H^δ . Following standard assumptions, we assume that v_L is decreasing with respect to both arguments.

Finally, we couple the dynamics of heavy vehicles with those of light vehicles. The interaction is obtained by introducing the dependence on ρ_L in the parameters Δ_{close} and Δ_{far} . More precisely, we introduce the increasing functions $\Delta_{\text{close}} = \Delta_{\text{close}}(\rho_L)$ and $\Delta_{\text{far}} = \Delta_{\text{far}}(\rho_L)$, and we denote by $A^C = A^C(X_k, X_{k+1}, V_k, V_{k+1}, \rho_L)$ the coupled acceleration defined as A in (18) and (19), with the new dependence on ρ_L .

We are now ready to present the fully coupled multi-scale model which reads as

$$\begin{cases} \begin{cases} \dot{X}_k = V_k \\ \dot{V}_k = A^C(X_k, X_{k+1}, V_k, V_{k+1}, \rho_L) \end{cases}, & k = 1, \dots, N - 1 \\ \partial_t \rho_L + \partial_x (\rho_L v_L(\rho_L, N_H^\delta)) = 0, & x \in \mathbb{R}, \quad t > 0. \end{cases} \quad (21)$$

To be coherent with our modeling assumptions, the functions Δ_{close} and Δ_{far} are constant for car densities below the transition level, i.e., $\rho_L \leq \rho_L^{\text{max}}/2$. In this case, the dynamics of trucks is independent from those of cars. Conversely, for $\rho_L > \rho_L^{\text{max}}/2$, we assume that the distances Δ_{close} and Δ_{far} increase linearly with respect to the average number of cars which are positioned between two trucks. This number can be easily computed considering the average number of cars in a road segment of length ℓ (equal to $\rho_L \ell$) and the number of trucks in the same road segment (assuming that all vehicles are uniformly distributed). We were unable to precisely calibrate the shape of the functions Δ_{close} and Δ_{far} from real data because it happens rarely that many cars are found between trucks: indeed, trucks tend to “push” cars into the fast lane rather than reacting to their presence.

3.3. Extension of the Models to General Road Networks

In order to perform a complete simulation on a generic network of highways, some important generalizations are needed.

3.3.1. Any Number of Lanes

Highways often have more than two lanes. Consider a road with n lanes of which n_H can be occupied by trucks. To allow the creeping phenomenon, we assume that $n_H < n$, which corresponds to $\rho_L^{\text{max}} \ell_L - \rho_H^{\text{max}} \ell_H > 0$ in terms of space occupied, cf. (8).

In the macroscopic approach, the model is easily generalized. Fundamental diagrams are modified in such a way that trucks start interacting with cars when the density of cars becomes greater than $\frac{n_H}{n} \rho_L^{\text{max}}$.

In the microscopic model, instead, an important modification is needed if $n_H > 1$. Indeed, in this case, trucks can overtake, and the microscopic model must be able to handle this. Typically, some new parameters are introduced in order to establish when a truck decides to overtake and if the truck can actually overtake, considering suitable safety constraints. From the computational point of view, additional difficulty arises when one has to find the truck in front of any other truck, since the ordering is lost whenever a truck overtakes. To make the search for the preceding vehicle computationally feasible, one can keep track, in a specific list, of all trucks located in each numerical cell and then update the list whenever a truck leaves or enters the cell.

3.3.2. Junctions

In order to perform a full simulation on a network of highways, both theoretical and numerical treatments of junctions are needed. Typically, highways do not have roundabouts, traffic lights or complex junctions; therefore, we can limit ourselves to handle simple merging (2 incoming roads and 1 outgoing road) and diverging (1 incoming road and 2 outgoing roads). We adopted the approach detailed in [13], in which the dynamics reformulated along paths and junctions “disappears”. The price to pay is that the number of equations is multiplied by the number of possible paths the drivers can follow at junctions.

In both merging and diverging, we have only two possible paths: for example, in the case of diverging, one can choose among the first and second outgoing roads, while in merging, one can decide to come from the first or the second incoming road.

Following this approach in the macroscopic model, the densities of each class of vehicles are split around every junction, ending up with a system of four conservation laws (two paths for each of the two classes of vehicles) with a discontinuous flux. After the junctions, densities are gathered together again, and the two-equation system (9) is restored.

In the multi-scale model, instead, the path-based approach is applied only for car dynamics since managing trucks is much simpler. Indeed, in the microscopic model, one can just move vehicles from one road to another on the basis of their destination, see [37]. Unfortunately, the ordering of trucks is lost every time a change of road takes place. In order to reduce the computational effort needed for the computation of the preceding truck of every truck, the same solution proposed in Section 3.3.1 can be applied.

4. Numerical Approximation and Calibration

In this section, we describe how the models introduced above can actually be implemented. First, we briefly recall the numerical methods we have adopted, and then we describe how we used real data to set the models' parameters.

4.1. Macroscopic Model

For the numerical approximation of the macroscopic model (9), we employ the extension of the *cell transmission model* (CTM) to the heterogeneous multi-class model proposed in [14]. Let Δx and Δt be the space and time steps, respectively, and let $(\rho_L^{n,i}, \rho_H^{n,i})$ be the traffic densities in the i th cell at the n th time step. The finite volume numerical scheme reads

$$\begin{cases} \rho_L^{n+1,i} = \rho_L^{n,i} + \frac{\Delta t}{\Delta x} (\mathcal{F}_L^{n,i-1/2} - \mathcal{F}_L^{n,i+1/2}) & (22a) \\ \rho_H^{n+1,i} = \rho_H^{n,i} + \frac{\Delta t}{\Delta x} (\mathcal{F}_H^{n,i-1/2} - \mathcal{F}_H^{n,i+1/2}) & (22b) \end{cases}$$

where

$$\mathcal{F}_L^{n,i+1/2} := \min \left\{ S_L(\rho_L^{n,i}, \rho_H^{n,i}), R_L(\rho_L^{n,i+1}, \rho_H^{n,i+1}) \right\}, \quad (23)$$

$$\mathcal{F}_H^{n,i+1/2} := \min \left\{ S_H(\rho_L^{n,i}, \rho_H^{n,i}), R_H(\rho_L^{n,i+1}, \rho_H^{n,i+1}) \right\}, \quad (24)$$

and $(S_L, R_L), (S_H, R_H)$ represent the sending and receiving functions of the two vehicle classes, respectively, defined by

$$\begin{aligned} S_L(\rho_L, \rho_H) &:= \begin{cases} f_L(\rho_L, \rho_H), & \text{if } \rho_L \leq \sigma_L(\rho_H), \\ f_L(\sigma_L(\rho_H), \rho_H), & \text{if } \rho_L > \sigma_L(\rho_H), \end{cases} \\ R_L(\rho_L, \rho_H) &:= \begin{cases} f_L(\sigma_L(\rho_H), \rho_H), & \text{if } \rho_L \leq \sigma_L(\rho_H), \\ f_L(\rho_L, \rho_H), & \text{if } \rho_L > \sigma_L(\rho_H), \end{cases} \end{aligned} \quad (25)$$

and similarly for (S_H, R_H) .

The numerical grid is chosen as $\Delta x = 100$ m and $\Delta t = 2.6$ s. The choice of the space step comes from the fact that the company Autovie Venete finds such granularity convenient for sharing traffic information to drivers, while the time step is dictated by the CFL condition.

Calibration of the fundamental diagrams was performed by fitting real data. We used all data measured in 2019 by one fixed sensor located near Cessalto, see Figures 9 and 10. Note that for high densities, the velocities drop rapidly to zero. Since we have no data for completely stationary vehicles under the sensor, we are not able to reconstruct data on high traffic density. For this reason, the maximal densities ρ_L^{\max} and ρ_H^{\max} are estimated by simply computing the ratio between the number of available lanes for the class and the average length of vehicles of that class, see Equation (6).

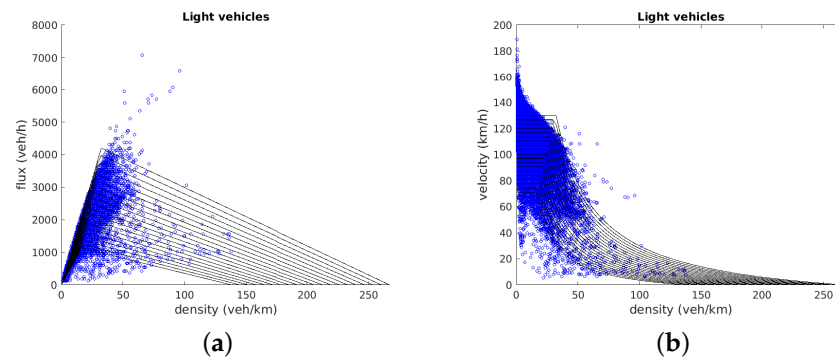


Figure 9. (a) Flux–density and (b) velocity–density relationships for cars with real data superimposed.

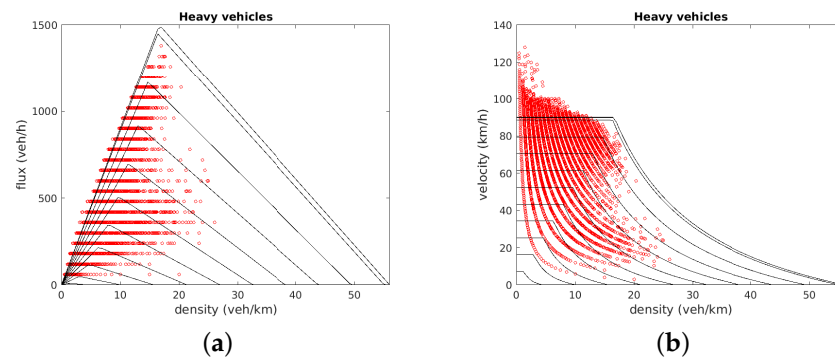


Figure 10. (a) Flux–density and (b) velocity–density relationships for trucks with real data superimposed.

Model parameters are summarized in Table 1. All functions which rule the dependence of ρ, v, f on the density of the other class are linear.

Table 1. Parameters for the macroscopic model.

	Light Vehicles	Heavy Vehicles
veh. length + safety dist. (km)	7.5×10^{-3}	18×10^{-3}
max max density (veh/km)	$\rho_L^*(0) = 267$	$\rho_H^*(0) = 56$
min max density (veh/km)	$\rho_L^*(\rho_H^{\max}) = 133$	$\rho_H^*(\rho_L^{\max}) = 0$
max max speed (km/h)	$v_L(0, 0) = 130$	$v_H(0, 0) = 90$
min max speed (km/h)	$v_L(0, \rho_H^{\max}) = 65$	$v_H(\rho_L^{\max}, 0) = 0$
max max flux (veh/h)	$f_L(\sigma_L(0), 0) = 4200$	$f_H(0, \sigma_H(0)) = 1500$
min max flux (veh/h)	$f_L(\sigma_L(\rho_H^{\max}), \rho_H^{\max}) = 1200$	$f_H(\rho_L^{\max}, \sigma_H(\rho_L^{\max})) = 0$

4.2. Multi-Scale Model

For the numerical approximation of the macroscopic part of the multi-scale model (21), we again employ scheme (22a), where N_H^δ plays the role of ρ_H in the obvious manner. The numerical grid is chosen as $\Delta x = 100$ m and $\Delta t = 2$ s.

The dependence of the flux on N_H^δ can generate some issues. For example, consider the case of no trucks and a car density $\hat{\rho}_L$ close to ρ_L^{\max} . When a truck enters the road, the maximal density allowed in the cell occupied by the truck drops to $\rho_L^*(N_H^\delta)$ according to (10). Now, if $\rho_L^*(N_H^\delta) < \hat{\rho}_L$, the current density $\hat{\rho}_L$ is found not to be compatible with the new maximal density. Although the entering truck perceives the cars, it is not guaranteed that the compatibility with the maximal density is respected at any time. To avoid this problem, trucks must be prevented from entering cells if the new maximal density caused by the presence of the truck itself is not compatible with current traffic conditions.

For the numerical approximation of the microscopic part, we used a standard Euler scheme with a time step of $\delta t = 0.1$ s. Note that this time step is much smaller than the time

step Δt used for the Godunov scheme, meaning that the updates of the trucks and cars are asynchronous.

Regarding the parameters, the macroscopic part of the model is treated as in Section 4.1 (Table 1). For the microscopic model, some parameters are easily calibrated by using real data and considering physical constraints. For example, V_H^{\max} was defined as in the macroscopic model. Δ_{far} was set in order to guarantee that trucks do not collide even in the event that a truck suddenly brakes with full power until it stops (note that our model allows, in principle, collisions since deceleration is bounded). Δ_{close} , instead, was set to a distance which guarantees catching the maximal observed density of trucks. In other words, when a queue of trucks is formed, the model predicts the correct maximal density.

Parameters τ_{acc} and τ_{dec} are, instead, more difficult to calibrate since they are not easily measurable. For those values, we considered a real stop and go wave observed by the company staff on 12 June 2017, generated by the slowdown of a truck near a bottleneck. The initial perturbation (slowdown) was amplified and, in a short time, generated a queue which propagated backwards. We run the microscopic model using real inflow data as left boundary conditions, and then we fitted the parameters in order to catch the real queue as measured in the field, see Figure 11.

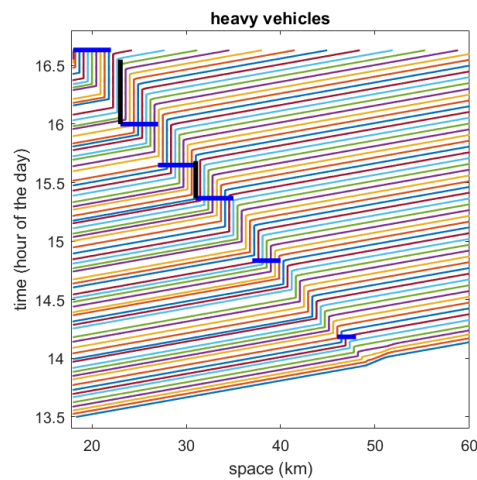


Figure 11. Simulated trajectories obtained with real inflow data as left boundary conditions (not all vehicles are plotted for visualization purposes). Horizontal blue lines and vertical black lines indicate, respectively, the position and the duration of the real queue as measured in the field.

The role of the parameters τ_{acc} and τ_{dec} is to adjust the points/times of the start and the end of the queue. We noted a strong sensitivity of the model to those parameters. As a consequence, it is quite difficult to catch the correct speed of the backward propagation of a queue when inertia comes into play. We summarize the values of the parameters in Table 2.

Table 2. Parameters for the microscopic model.

δ	50×10^{-3}	km
Δ_{close}	25×10^{-3}	km
Δ_{far}	50×10^{-3}	km
V_H^{\max}	90	km/h
τ_{dec}	2×10^{-4}	h
τ_{acc}	1.4×10^{-2}	h

5. Numerical Results

In this section, we present the numerical results obtained with models (9) and (21).

5.1. Macroscopic Model

Here, we present three tests which highlight how the macroscopic model reproduces some interesting phenomena arising from the coupled dynamics of cars and trucks. In particular, we focus on the creeping phenomenon, the shared occupancy and the stop and go waves.

5.1.1. Test 1A: Creeping

In this simple test, we observe the creeping phenomenon, see Figure 12. The simulation starts with a constant density $(\rho_L, \rho_H) = (10, 13)$ veh/km all along the road. At the end of the road (right boundary), trucks are stopped by fixing their density at its maximum value $\rho_H^{\max} = 56$: a queue of trucks propagates backward from the end of the road, while a constant flux of cars approaches the beginning of the queue. Once cars reach the trucks' queue, they have to slow down but do not stop completely. More precisely, the cars' velocity drops to 65 km/h. Note that the car density remains under the transition level, and then the dynamics is in the partial coupling phase all the time. Moreover, cars are always in the freeflow regime and then move at maximal speed, but the maximal speed changes as a function of the truck density.

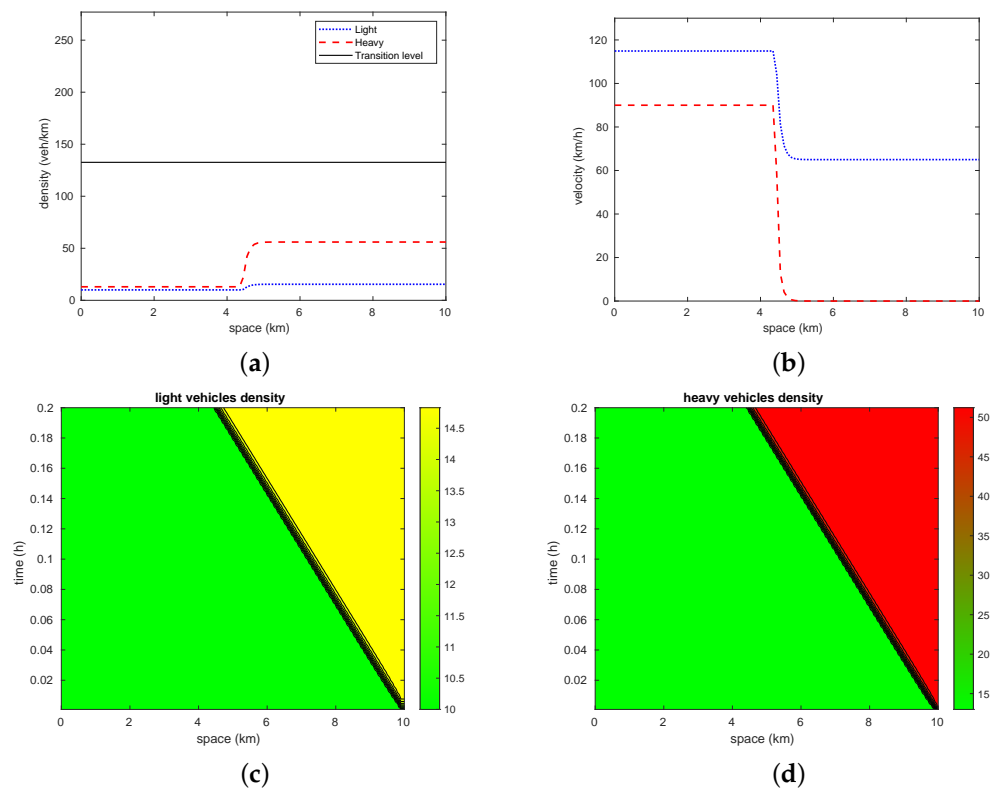


Figure 12. Test 1A: (a) Density and (b) velocity of light and heavy vehicles as a function of space at final time. (c) Density of light and (d) heavy vehicles in space–time.

5.1.2. Test 2A: Cars' Congestion Affects Truck Dynamics

In this test, we observe the effect of congestion of cars, see Figure 13. The simulation starts with a constant density $(\rho_L, \rho_H) = (10, 8)$ veh/km all along the road. At the end of the road (right boundary), the density of cars is fixed to 186 veh/km to create the slowdown. The car density is larger than the transition level, so cars have to invade the slow lane. Trucks facing the car congestion slow down but do not just occupy the space left to them by cars; rather, they conquer some extra space, thus decreasing the car density. As a result, both cars and trucks proceed slowly without stopping, and the initial car congestion propagates backward with a density lower than the transition level.

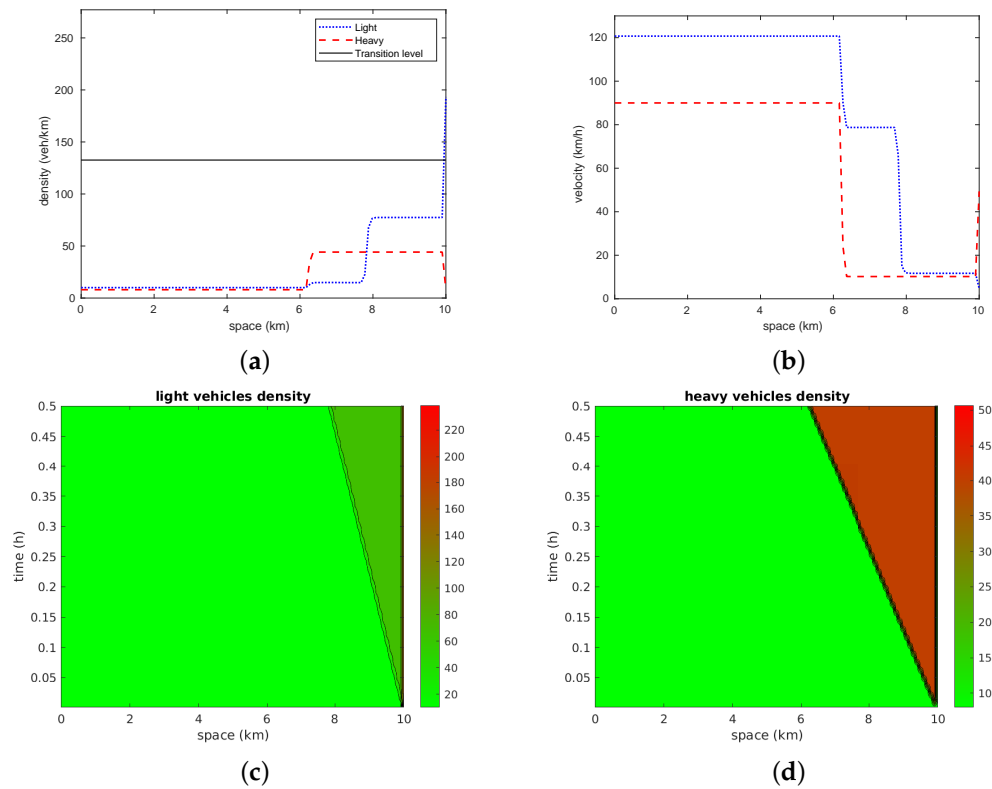


Figure 13. Test 2A: (a) Density and (b) velocity of light and heavy vehicles as a function of space at final time. (c) Density of light and (d) heavy vehicles in space–time.

5.1.3. Test 3A: Stop and Go Wave

In this test, we study the evolution of a small perturbation in the truck density, see Figure 14. At the initial time, the truck density is constant and equal to 12 veh/km, except for a small perturbation at the end of the road where the density is equal to 30 veh/km. The car density instead oscillates just above the transition level. It is plain that a single-class LWR model for trucks only would flatten the perturbation in a short time. Conversely, in this case, the coupling with car dynamics causes the perturbation to propagate backward without vanishing. This second-order-type effect is obtained thanks to the fact that the fundamental diagram of trucks is continuously modified by the oscillating car density.

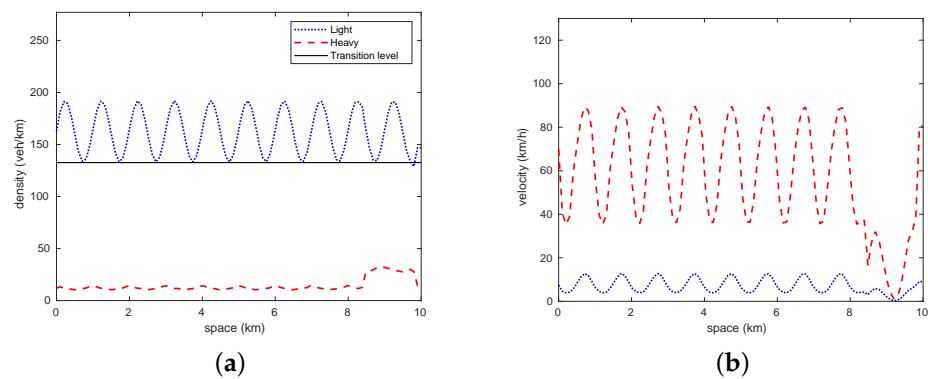


Figure 14. Cont.

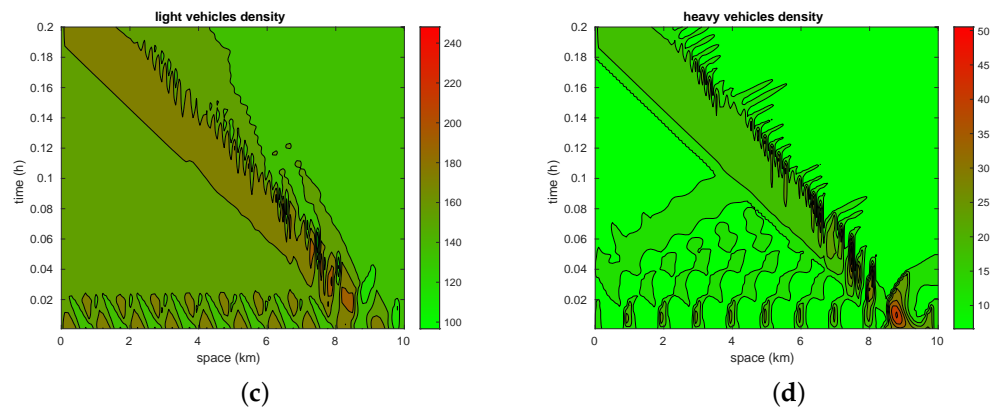


Figure 14. Test 3A: (a) Density and (b) velocity of light and heavy vehicles as a function of space at $t = \Delta t$ (i.e., just after the initial time). (c) Density of light and (d) heavy vehicles in space–time. The evolution of the initial perturbation in the truck density starting at 9 km is perfectly visible, which creates, in turn, a perturbation in the car density.

5.2. Multi-Scale Model

Here, we replicate, with the multi-scale model, the first two scenarios already investigated in Section 5.1. The third scenario was already considered in Figure 11, where the second-order microscopic model is able to reproduce stop and go waves alone, without the need to couple car dynamics. Finally, we consider the case of a merge.

5.2.1. Test 1B: Creeping Effect

Similar to Test 1A in Section 5.1.1, here, one truck stops completely and creates a long queue of trucks behind, which saturates the slow lane. When cars reach the truck queue, they all move to the fast lane staying at the (new, reduced) maximal velocity of 65 km/h, see Figure 15.

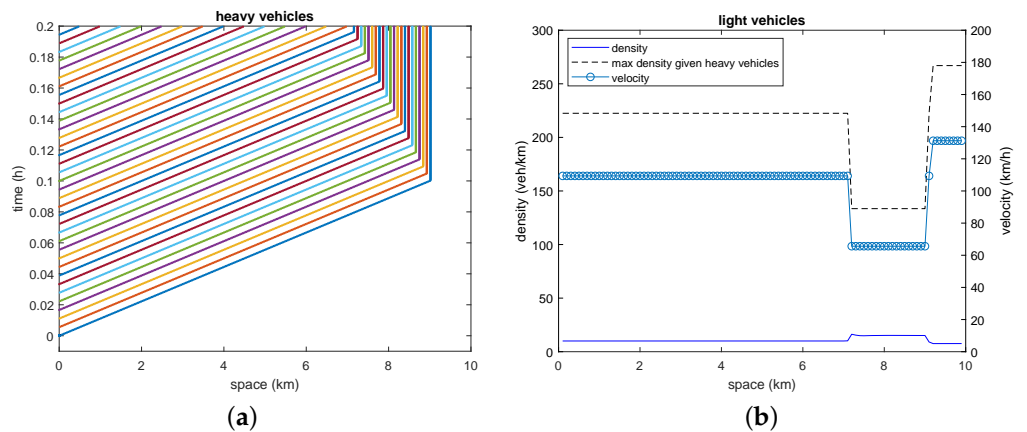


Figure 15. Test 1B: (a) Trajectories of trucks in space–time (for visualization purposes, not all trucks are actually plotted). When the first truck stops, a queue is formed behind. (b) Car density, car velocity and car maximal density given the number of trucks at final time. Creeping is visible between 7 and 9 km.

5.2.2. Test 2B: Cars’ Congestion Affects Truck Dynamics

Similar to Test 2A in Section 5.1.2, congestion of cars at the end of the road slows down trucks, see Figure 16. The results are similar to those obtained by the macroscopic model, but here, trucks stop completely, forming a queue.

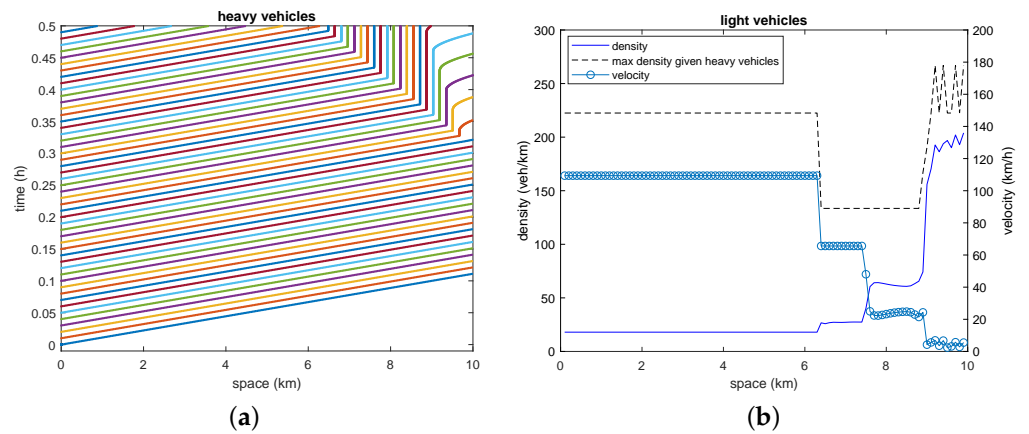


Figure 16. Test 2B: (a) Trajectories of trucks in space–time (for visualization purposes, not all trucks are actually plotted). They stop for a while and then accelerate. (b) Car density, car velocity and car maximal density given the number of trucks at final time.

5.2.3. Test 3B: Merge

In this test, we consider a merge (two incoming roads and one outgoing road). At time $t = 0$, the three roads are empty. A constant inflow of trucks (one every 4 s) comes from the left boundary of both incoming roads, while a constant density of cars ($\rho_L = 32$) is imposed as a Dirichlet left boundary condition on the second incoming road only. The first incoming road has no cars. When trucks reach the junction and merge, they suddenly break and rapidly form a queue which propagates backward along both incoming roads, see Figure 17a,b.

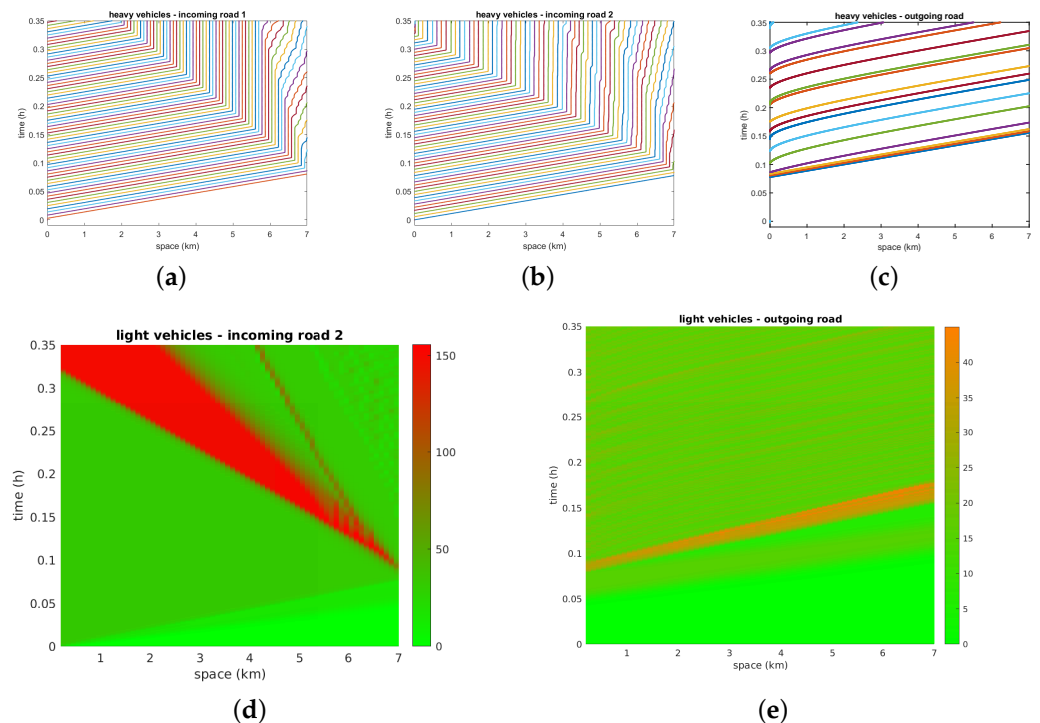


Figure 17. Test 3B: (a–c) Trajectories of trucks in space–time on the first incoming road, second incoming road and outgoing road, respectively (for visualization purposes, not all trucks are actually plotted). (d,e) Car density on second incoming road and outgoing road, respectively.

Queues are not identical due to the presence of cars along the second incoming road. One can note that when the trucks downstream of the queue start moving again, their flux is not maximal: indeed, if the flow were maximum, a queue at the junction would

immediately reform as it happened in the first place. This is the well-known *capacity drop* phenomenon, ruled by τ_{acc} , cf. [38]. As a consequence, trucks are able to cross the junction without spillback. Cars, instead, move at the maximal flux until they encounter the truck queue. The queue acts as a moving bottleneck and drops the road capacity; therefore, the car traffic immediately enters the congested state, and the density increases. Downstream, the density remains in the freeflow state, and cars cross the junction without spillback, see Figure 17d,e.

6. Conclusions and Future Work

In this paper, we presented two models for two-class traffic flow. Although the models are tailored for a specific case study, they are sufficiently general to be useful in other motorways. Moreover, both models can be easily generalized to more than two classes of vehicles and a different ratio between the number of lanes used by trucks and the number of lanes used by cars.

We have shown that the models are able to reproduce, both qualitatively and quantitatively, some notable traffic phenomena arising from the interactions of the two classes. Interestingly, the macroscopic model, although purely first-order, is able to reproduce stop and go waves thanks to the coupling of the two classes.

After this preliminary analysis, it is possible to sketch some conclusions about the advantages and drawbacks of the two models: The multi-scale model has a greater potential since the second-order microscopic part makes it more realistic and then suitable for quantitative predictions. Nevertheless, the macroscopic model appears to be simpler and more manageable, thus representing a valid alternative if one wants to avoid tracking all single vehicles, especially for saving computational time.

In conclusion, we believe that both the proposed models represent the best compromise between accuracy and implementability. In fact, decoupling the dynamics of different classes excessively simplifies the problem description and does not allow obtaining an accurate forecast; conversely, moving to second-order macroscopic models or including multi-lane features in the models notably increases the complexity of the code as well as the number of parameters to be tuned. These generalizations would allow, in principle, easily catching inertia-based phenomena in all classes of vehicles and tracking the density of *each class* of vehicle in *each lane*, but, in our opinion, they make that model unfeasible for practical applications.

In the future, we plan to improve the models including the possibility that they are fed by both Lagrangian (GPS-like) and Eulerian data coming from mobile and fixed sensors, respectively, cf. [39]. Moreover, we plan to estimate, in real time, the difference between predicted and measured densities using the machinery developed in [13], hopefully creating an algorithm for the auto-calibration of the models in real time.

Author Contributions: Conceptualization, M.B. and E.C.; data curation, P.R.; funding acquisition, M.B., E.C. and P.R.; investigation, M.B., E.C. and P.R.; methodology, M.B. and E.C.; visualization, M.B. and E.C.; writing—original draft, M.B. and E.C.; writing—review and editing, M.B., E.C. and P.R. All authors have read and agreed to the published version of the manuscript.

Funding: This work was partially funded by the company Autovie Venete S.p.A. This work was also carried out within the research project “SMARTOUR: Intelligent Platform for Tourism” (No. SCN_00166) funded by the Ministry of University and Research with the Regional Development Fund of European Union (PON Research and Competitiveness 2007–2013). The authors also acknowledge the Italian Minister of Instruction, University and Research for supporting this research with funds coming from the project entitled *Innovative numerical methods for evolutionary partial differential equations and applications* (PRIN Project 2017, No. 2017KKJP4X). M.B. and E.C. are members of the INdAM Research group GNCS.

Data Availability Statement: Data are not publicly available.

Acknowledgments: The authors want to thank all the Autovie Venete staff as well as Gabriella Bretti, Matteo Piu, Elisa Iacomini, Caterina Balzotti and Elia Onofri for valuable help.

Conflicts of Interest: The authors declare no conflict of interest.

References

- Lighthill, M.J.; Whitham, G.B. On kinematic waves II. A theory of traffic flow on long crowded roads. *Proc. R. Soc. Lond. Ser. A* **1955**, *229*, 317–345. [[CrossRef](#)]
- Richards, P.I. Shock waves on the highway. *Oper. Res.* **1956**, *4*, 42–51. [[CrossRef](#)]
- Cristiani, E.; Iacomini, E. An interface-free multi-scale multi-order model for traffic flow. *Discret. Contin. Dyn. Syst. Ser. B* **2019**, *24*, 6189–6207. [[CrossRef](#)]
- Garavello, M.; Piccoli, B. *Traffic Flow on Networks*; American Institute of Mathematical Sciences: Springfield, MO, USA, 2006.
- Coclite, G.M.; Garavello, M.; Piccoli, B. Traffic flow on a road network. *SIAM J. Math. Anal.* **2005**, *36*, 1862–1886. [[CrossRef](#)]
- Holden, H.; Risebro, H. A mathematical model of traffic flow on a network of unidirectional roads. *SIAM J. Math. Anal.* **1995**, *26*, 999–1017. [[CrossRef](#)]
- Bressan, A.; Nguyen, K.T. Conservation law models for traffic flow on a network of roads. *Netw. Heterog. Media* **2015**, *10*, 255–293. [[CrossRef](#)]
- Garavello, M.; Goatin, P. The Cauchy problem at a node with buffer. *Discret. Contin. Dyn. Syst. Ser. A* **2012**, *32*, 1915–1938. [[CrossRef](#)]
- Herty, M.; Lebacque, J.P.; Moutari, S. A novel model for intersections of vehicular traffic flow. *Netw. Heterog. Media* **2009**, *4*, 813–826. [[CrossRef](#)]
- Bretti, G.; Briani, M.; Cristiani, E. An easy-to-use algorithm for simulating traffic flow on networks: Numerical experiments. *Discret. Contin. Dyn. Syst. Ser. S* **2014**, *7*, 379–394. [[CrossRef](#)]
- Briani, M.; Cristiani, E. An easy-to-use algorithm for simulating traffic flow on networks: Theoretical study. *Netw. Heterog. Media* **2014**, *9*, 519–552. [[CrossRef](#)]
- Hilliges, M.; Weidlich, W. A phenomenological model for dynamic traffic flow in networks. *Transp. Res. Part B* **1995**, *29*, 407–431. [[CrossRef](#)]
- Briani, M.; Cristiani, E.; Iacomini, E. Sensitivity analysis of the LWR model for traffic forecast on large networks using Wasserstein distance. *Commun. Math. Sci.* **2018**, *16*, 123–144. [[CrossRef](#)]
- Fan, S.; Work, D.B. A heterogeneous multiclass traffic flow model with creeping. *SIAM J. Appl. Math.* **2015**, *75*, 813–835. [[CrossRef](#)]
- van Wageningen-Kessels, F. Framework to assess multiclass continuum traffic flow models. *Transp. Res. Rec.* **2016**, *2553*, 150–160. [[CrossRef](#)]
- (Sean) Qian, Z.; Li, J.; Li, X.; Zhang, M.; Wang, H. Modeling heterogeneous traffic flow: A pragmatic approach. *Transp. Res. Part B* **2017**, *99*, 183–204. [[CrossRef](#)]
- Ferrara, A.; Sacone, S.; Siri, S. *Freeway Traffic Modelling and Control*; Springer: Berlin/Heidelberg, Germany, 2018.
- Kessels, F. *Traffic Flow Modelling*; Springer: Berlin/Heidelberg, Germany, 2019.
- Agarwal, A.; Lämmel, G. Modeling seepage behavior of smaller vehicles in mixed traffic conditions using an agent based simulation. *Transp. Dev. Econ.* **2016**, *2*, 8. [[CrossRef](#)]
- Benzoni-Gavage, S.; Colombo, R.M. An n -populations model for traffic flow. *Eur. Jnl Appl. Math.* **2003**, *14*, 587–612. [[CrossRef](#)]
- Balzotti, C.; Göttlich, S. A two-dimensional multi-class traffic flow model. *Netw. Heterog. Media* **2021**, *16*, 69–90. [[CrossRef](#)]
- Fan, S.; Seibold, B. Data-fitted first-order traffic models and their second-order generalizations. Comparison by trajectory and sensor data. *Transp. Res. Rec.* **2013**, *2391*, 32–43. [[CrossRef](#)]
- Fan, S.; Herty, M.; Seibold, B. Comparative model accuracy of a data-fitted generalized Aw-Rascle-Zhang model. *Netw. Heterog. Media* **2014**, *9*, 239–268. [[CrossRef](#)]
- Klar, A.; Günther, M.; Wegener, R.; Materne, T. Multivalued fundamental diagrams and stop and go waves for continuum traffic flow equations. *SIAM J. Appl. Math.* **2004**, *64*, 468–483. [[CrossRef](#)]
- Herty, M.; Illner, R. Coupling of non-local driving behaviour with fundamental diagrams. *Kinet. Relat. Models* **2012**, *5*, 843–855. [[CrossRef](#)]
- Ni, D.; Hsieh, H.K.; Jiang, T. Modeling phase diagrams as stochastic processes with application in vehicular traffic flow. *Appl. Math. Model.* **2018**, *53*, 106–117. [[CrossRef](#)]
- Paipuri, M.; Leclercq, L. Bi-modal macroscopic traffic dynamics in a single region. *Transp. Res. Part B* **2020**, *133*, 257–290. [[CrossRef](#)]
- Puppo, G.; Semplice, M.; Tosin, A.; Visconti, G. Fundamental diagrams in traffic flow: The case of heterogeneous kinetic models. *Commun. Math. Sci.* **2016**, *14*, 643–669. [[CrossRef](#)]
- Visconti, G.; Herty, M.; Puppo, G.; Tosin, A. Multivalued fundamental diagrams of traffic flow in the kinetic Fokker–Planck limit. *Multiscale Model. Simul.* **2017**, *15*, 1267–1293. [[CrossRef](#)]
- Wang, H.; Ni, D.; Chen, Q.Y.; Li, J. Stochastic modeling of the equilibrium speed-density relationship. *J. Adv. Transp.* **2013**, *47*, 126–150. [[CrossRef](#)]
- Fan, S.; Sun, Y.; Piccoli, B.; Seibold, B.; Work, D.B. A collapsed generalized Aw-Rascle-Zhang model and its model accuracy. *arXiv* **2017**, arXiv:1702.03624.
- Bretti, G.; Cristiani, E.; Lattanzio, C.; Maurizi, A.; Piccoli, B. Two algorithms for a fully coupled and consistently macroscopic PDE-ODE system modeling a moving bottleneck on a road. *Math. Eng.* **2018**, *1*, 55–83. [[CrossRef](#)]

33. Zhao, Y.; Zhang, H.M. A unified follow-the-leader model for vehicle, bicycle and pedestrian traffic. *Transp. Res. Part B* **2017**, *105*, 315–327. [[CrossRef](#)]
34. Colombo, R.M. Hyperbolic phase transitions in traffic flow. *SIAM J. Appl. Math.* **2002**, *63*, 708–721. [[CrossRef](#)]
35. Colombo, R.M.; Goatin, P.; Piccoli, B. Road networks with phase transitions. *J. Hyperbolic Differ. Eq.* **2010**, *7*, 85–106. [[CrossRef](#)]
36. Delle Monache, M.L.; Chi, K.; Chen, Y.; Goatin, P.; Han, K.; Qiu, J.; Piccoli, B. Three-phase fundamental diagram from three-dimensional traffic data. *Axioms* **2021**, *10*, 17. [[CrossRef](#)]
37. Cristiani, E.; Sahu, S. On the micro-to-macro limit for first-order traffic flow models on networks. *Netw. Heterog. Media* **2016**, *11*, 395–413. [[CrossRef](#)]
38. Calvert, S.C.; van Wageningen-Kessels, F.L.M.; Hoogendoorn, S.P. Capacity drop through reaction times in heterogeneous traffic. *J. Traffic Transp. Eng.* **2018**, *5*, 96–104. [[CrossRef](#)]
39. Colombo, R.M.; Marcellini, F. A traffic model aware of real time data. *Math. Models Methods Appl. Sci.* **2016**, *26*, 445–467. [[CrossRef](#)]